University of Baghdad
College of Engineering
JOURNAL OF ENGINEERING

Journal of Engineering
journal homepage: www.joe.uobaghdad.edu.iq
Volume 28 Number 10 October 2022

Mechanical and Energy Engineering

Numerical Study of Thermal Conductivity Effect on The Performance of Thermal Energy Storage

Hassan Hadi Sadiq
MSc. Student
Department of Mechanical Engineering
College of Engineering
University of Baghdad
Baghdad, Iraq
h.alebadi1303@coeng.uobaghdad.edu.iq

Munther Abdullah Mussa
Assist prof.
Department of Mechanical Engineering
College of Engineering
University of Baghdad
Baghdad, Iraq.
munther@coeng.uobaghdad.edu.iq

Abstract

In this study, the effect of the thermal conductivity of phase change material (PCM) on the performance of thermal energy storage has been analyzed numerically. A horizontal concentric shell-and-tube latent heat thermal energy storage system (LHTESS) has been performed during the solidification process. Two types of paraffin wax with different melting temperatures and thermal conductivity were used as a PCM on the shell side, case1=0.265W/m.K and case2=0.311 W/m.K. Water has been used as heat transfer fluid (HTF) flow through in tube side. Ansys fluent has been used to analyze the model by taking into account phase change by the enthalpy method used to deal with phase transition. The numerical simulation assumptions were three-dimensional, transient, and laminar flow was used. The result for the PCMs of performance, temperature distribution, and liquid fraction during the discharge process were compared to each other. Furthermore, the Nusselt number was analyzed. The result showed that the increase in thermal conductivity of PCM reduces the time of the solidification process by 20%. The performance of LHTESS for case 2 is 63.2%, whereas for case1 is 54.6%.

Keywords: thermal performance, thermal conductivity effect, solidification, shell and tube

دراسة عددية حول الموصلية و تاثيرها على كفاءة المستودع الحراري

حسن هادي صادق
طالب الماجستير
كلية الهندسة – جامعة بغداد

منذر عبد الله موسى
أستاذ مساعد
كلية الهندسة – جامعة بغداد

*Corresponding author
Peer review under the responsibility of University of Baghdad.
https://doi.org/10.31026/j.eng.2022.10.05

Article received: 27/4/2022
Article accepted: 5/8/2022
Article published: 1/10/2022

الخلاصة

في هذه الدراسة، تم إجراء تحليل عددي لنظام تخزين الطاقة الحرارية الحرارية الكامنة في مبادل حراري أثناء عملية التبريد. تم تحليل تأثير الموصلية الحرارية لمادة تغيير الطور على أداء تخزين الطاقة الحرارية. تم استخدام نوعين من شمع البارافين بدرجات حرارة انصهار مختلفة وموصلية حرارية case2 = 0.311 W/ m.K,case1 = 0.265W / m.K . تم استخدام الماء كسائل للتبريد. تم استخدام برنامج Ansys لتحليل النموذج. أظهرت النتائج أن زيادة الموصلية الحرارية للمواد المتغيرة الطور يقلل من وقت عملية التصلب بنسبة 20٪. الكفاءة لـ case2 هو 63.2٪ بينما بالنسبة للحالة 1 هو 54.

الكلمات الرئيسية: أداء تخزين الطاقة الحرارية، تأثير الموصلية الحرارية، التصلب، مبادل حراري

1. INTRODUCTION

Solar energy is a promising and favorable renewable energy. Utilizing solar energy is limited due to the intermittent nature of the sun and the weather's effect on it. Latent heat thermal energy storage (LHTES) appears as a promising solution due to its high performance, reliability, high storage density, and closely constant temperature of energy delivery. The main drawback of LHTES is that the PCM used in the system has low thermal conductivity. That means low charging and discharging rates. For this reason, many enhancement techniques of heat transfer are adopted, like adding fin, nanomaterial, or using a highly conductive material. It is well known that high thermal conductivity reduces the time of melting and solidification.

(Joudi and Taha, 2012) investigated the storage of energy and energy regeneration through charge/discharge processes. They used four types of Paraffins. They investigated different parameters such as the shape of the container, the mass of PCM, different mass flow of HTF, and temperature difference between PCM and HTF. Their Result showed that the PCMs in a cylindrical vessel melt and solidify faster than in a square vessel. Also, the mass flow rate and temperature difference increase reduce the time required for complete phase change. **(Li and Wu, 2015)** inspected the impact of extended fin and PCM/expanded graphite on the performances of TES units. Synthetic oil, molten salts, and $NaNO_3$ were used as HTFs and PCM, respectively. They showed that the full melting and solidification time could be reduced by at least 14%, whereas using the composite PCM materials can shorten the time by at least 20%. Furthermore, they concluded that the composite is a more effective way to improve the heat performance of the TES system than the extended fin. **(Kadim, 2015)** studied the enhancement of heat transfer of PCM through charging and discharging processes. They added highly conductive material copper in the form of brushes. It is installed on both sides of PCM and air. They tested different void fractions of brushes and different air velocities. Their result showed that the minimum void fraction of brush gave the higher heat transfer in PCM and reduced the time for

melting up to 4.49 times as compared with the case of no brush. In addition, they found that the addition of brushes in air side minimize the discharge time and increase the convection heat transfer coefficient as the brush void fraction decreases. Furthermore, the minimum velocity of air gave a higher outlet temperature. **(Kuboth et al., 2017)** performed an investigation of utilizing circular fin and its influence on the performance of LHTESS. They used paraffin wax and water as a PCM and HTF, respectively. Their results showed an influence of fin allocation on storage performance. In addition, the average storage performance at the total discharge only increased by 3% with the best allocation compared to an equidistant arrangement. **(Yang et al., 2017)** numerically investigated thermal performance in a shell-and-tube LHTES unit with annular fins. They used commercial grade paraffin as PCM and water as HTF. They demonstrated that the performance enhancement of the full melting time could be maximally reduced by 65% by inserting annular fins into PCM. **(Bhagat et al., 2018)** numerically estimated the performance of LHTESS. Shell and finned multi-tube LHTES for medium temperature (~200 °C) solar thermal power plant had been used. They used A164 with a melting temperature of 168.7 °C, and thermic oil Hytherm of 600 was used as a PCM and HTF, respectively. In their study, a thermal conductivity enhancer in the form of a fin had been used to enhance heat transfer in the PCM. They found that the number of fins and fin thickness significantly affected the thermal performance of the storage system. Also, enhancement in heat transfer for high thermal conductivity material fin was marginal. **(Parsazadeh and Duan, 2018)** presented multiscale heat transfer enhancement technique, with circular plate fins on the outer surface of HTF tube and highly conductive nanoparticles (Al_2O_3). A numerical study was performed on a shell and tube thermal energy storage unit using a common organic PCM paraffin wax. They showed that the fin angle and nanoparticle concentration are two significant parameters affecting PCM melting. They concluded that adding nanoparticles to the PCM does not accelerate the charging process. Nevertheless, the nanoparticles lead to a longer charging time and lower overall heat transfer rate. The positive fin angles are found to be favorable for PCM melting. **(Tao et al., 2019)** examined the impact of nanomaterial on heat storage performance of nano composite-PCM. The melting behavior of pure PCM and four kinds of nano additives in a horizontal concentric tube were investigated. Their main result showed that thermal conductivity and melting temperature significantly affect PCM melting rate and average heat storage rate. **(Liu et al., 2020)** investigated a shell-and-tube heat exchanger. Thermal performance of multiple shell-and-tube, two-dimensional and transient heat transfer was simulated. Sensible TES using graphite, latent TES using PCMs, and a hybrid of both had been used.

They found that the single graphite has fewer issues. Nevertheless, single graphite has the lowest storage density. Their conclusion showed that the hybrid PCM- graphite-PCM has a higher energy density and storage effectiveness of 70.7%. **(Shi et al., 2020)** studied the effect of magnetic field on the performance of LHTESS during the charging and discharging process. Quadrupole magnets, Paraffin A16 with a melting temperature point of 16 ^{o}C as a PCM and Fe_3O_4 nanoparticles had been used. They concluded that the performance enhancement of the decrease in full charging time and full discharging time by applying the magnetic field with an intensity of B0=50mT is 80.02% and 53.19% respectively. **(Nóbrega et al., 2021)** numerically calculated thermal performance during the solidification process and they compared the use of with/without fin-tube and nanomaterial. Al_2O_3 nanoparticles had been used with different percentages of 1-10%. Their result showed that in case of adding 10% of Al_2O_3 to PCM with a fin-tube will reduces the complete solidification time by 9.1% compare to the result of the finless tube and pure PCM. **(Pu et al., 2021)** investigated the heat transfer performance of shell and tube numerically. Multiple PCMs and single PCM, in addition to three types of gradient copper foam positive gradient, non-gradient, and negative gradient, have been used to accelerate the melting of PCMs and improve the heat transfer effectiveness. The results indicated that the utilization of a single PCM showed better effect than that of multiple radial PCMs. Also, the negative gradient offers better heat transfer effectiveness than the two other types. The complete melting time saving was up to 87.5%. However, the temperature distribution of non-gradient type was more uniform compared to positive and negative types. **(Fathi and Mussa, 2021)** studied the influence of the tube rotation with 9 rpm on the melting process. Shell and tube LHTESS were adopted for numerical investigation. Paraffin wax was used as a PCM and water as an HTF. Their result showed that the enhancement in liquid content was 3.5% for 6 hours charging process.

In the present study, the effect of the thermal conductivity of PCM on thermal performance during the solidification process will be investigated. Two kinds of paraffin wax as PCM with different thermal conductivity will be used. Mass fraction, temperature distribution, and efficiency of LHTESS will be discussed. The main finding in the current study is that the performance of LHTESS increased when the average temperature and liquid fraction decreased. The theoretical efficiency during the discharge process for case 2 is 63.2%, whereas for case1 is 54.6%

2. Physical model

2.1 System description

In this study, the investigation model consists of a horizontal concentric double pipe shell and tube LHTESS, as shown in **Figure 1**. The HTF is water that flows through the inner side of the tube. Two paraffin wax adopted in this study with different thermal conductivity, Iraqi paraffin (case1) and commercial paraffin (case2). The wax filled in the space of the shell side. The outer diameter of the shell which is made from aluminum, is 100 mm, and its thickness is 10 mm. The inner diameter of the HTF tube which is made from copper, is 26 mm, and its thickness is 1 mm. During the discharge process, the HTF temperature and mass flow rate are considered constant at 296 K and 2 l/min, respectively. Thermophysical properties of PCMs as shown in **Figure 1.**

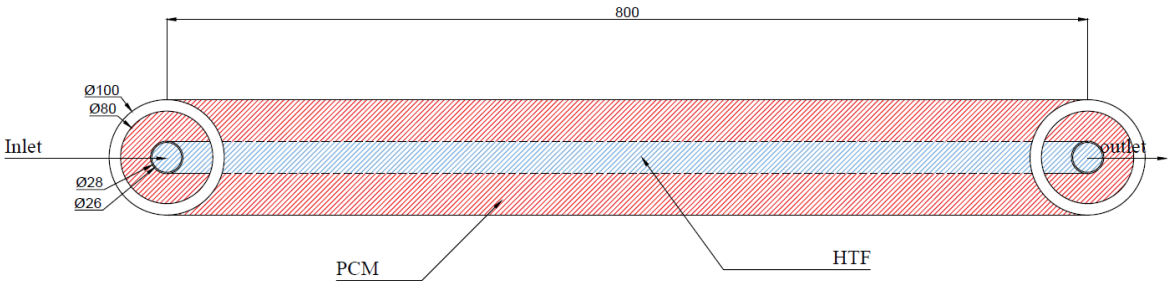

Figure 1 Schematic diagram of the model (all dimension in mm)

Thermal conductivity was measured experimentally at the University of Technology - Department of Material Engineering.

Table 1 Thermophysical properties of PCMs

Material	Properties						
	ρ_{solid} (kg/m^3)	ρ_{liquid} (kg/m^3)	C_p (J/kg·K)	k (W/m·K)	L (J/kg)	Melting temp. (K)	μ (kg/m·s)
Iraqi paraffin	852.14	766.11	2900	0.265	270715	334	0.0188
Commercial paraffin	813.795	733.33	2104	0.311	219290	331	0.0236
Water	-	998.2	4182	0.6	-	-	0.001003

2.2 Assumption of Equation and Boundary conditions

The following assumptions were adopted to solve the governing equation:

- HTF is considered incompressible and laminar.
- The HTF inlet of temperature and velocity constantly settled at 296K and 2 l/min flow.
- Thermophysical properties are constant.
- The PCM in liquid phase through discharge process with temperature 340K.
- The outer surface of the shell is insulated.
- Viscous dissipation is negligible.
- The boussinesq approximation was employed for the variant in density.

2.3 Governing equation

The simulation of thermal performance of horizontal concentric shell and tube was done based on the enthalpy porosity method **(Al-Abidi et al., 2013)**. Conservation of energy can be demonstrated in terms of total volumetric enthalpy and temperature for constant thermophysical properties **(Seddegh et al., 2016)**:

$$\frac{\partial \rho H}{\partial t} + \nabla \cdot (\rho v H) = \nabla \cdot (k \nabla T) + S \quad (1)$$

where ρ is the PCM density, ν is the velocity, k is thermal conductivity, S is a source term, and H is the total volumetric enthalpy. Total volumetric of enthalpy can be expressed in terms of summation sensible and latent heats as:

$$\boldsymbol{H = h + \gamma L} \quad (2)$$

$$\boldsymbol{h = h_{ref} + \int_{T_{ref}}^{T} C_p\, dT} \quad (3)$$

Where L is the latent heat, h_{ref} is the sensible heat, T_{ref} is the reference temperature, and c_p is specific heat. γ is a liquid fraction which is the fraction of cell volume. The mushy zone is a region where the liquid fraction lies between 0 and 1 and can be expressed as:

$$\boldsymbol{\gamma} = \begin{cases} \mathbf{0} & \boldsymbol{T<T_{solidus}} \\ \dfrac{\boldsymbol{T-T_{solidus}}}{\boldsymbol{T_{liquidus}-T_{solidus}}} & \boldsymbol{T_{solidus}\le T\le T_{liquidus}} \\ \mathbf{1} & \boldsymbol{T>T_{liquidus}} \end{cases} \quad (4)$$

Substitution eq. (2)-(4) in eq. (1), the energy equation becomes as:

$$\boldsymbol{\frac{\partial \rho h}{\partial t} + \nabla \cdot (\rho v h) = \nabla \cdot (k \nabla T) - \frac{\partial \rho \gamma L}{\partial t} - \nabla \cdot (\rho v \gamma L) + S} \quad (5)$$

Momentum equation becomes as:

$$\boldsymbol{\frac{\partial \rho v}{\partial t} + \nabla \cdot (\rho v v) = -\nabla P + \nabla \cdot (\mu \nabla v) + \rho g + \frac{(1-\gamma)^2}{\gamma^3+\varepsilon} v A_{mush}} \quad (6)$$

Where v is the velocity, A_{mush} is the mushy zone constant, which varies between 104-107; this study considered 10^5. ε is a constant to avoid the division on zero, which is equal to $\varepsilon = 0.001$ **(Al-Abidi et al., 2013)**. The Boussinesq approximation is used when the variation in density is small. So, the momentum equation becomes as:

$$\boldsymbol{\frac{\partial \rho_0 v}{\partial t} + \nabla \cdot (\rho_0 v v) = -\nabla P + \nabla \cdot (\mu \nabla v) + (\rho - \rho_0) g + \frac{(1-\gamma)^2}{\gamma^3+\varepsilon} v A_{mush}} \quad (7)$$

$$\boldsymbol{(\rho - \rho_0) = -\rho_0 \beta (T - T_0)} \quad (8)$$

where ρ_0 is the reference density, T_0 temperature and β the volumetric expansion coefficient. The continuity is given as:

$$\boldsymbol{\frac{\partial \rho}{\partial t} + \nabla \cdot (\rho v) = 0} \quad (9)$$

2.4 Performance calculation

In this study, the instantaneous energy (q) in addition to accumulative energy (Q), which is gained or realized by water as HTF throughout the charging and discharging process, can be described by as **(Hosseini et al., 2014)** :

$$q_{ch} = \dot{m} c_p (T_{in} - T_{out}) \quad (10)$$

$$q_{dis} = \dot{m} c_p (T_{out} - T_{in}) \quad (11)$$

$$Q_{ch\&dis} = \sum q_{ch\&dis} \Delta t \quad (12)$$

where ($\dot{m}$), (c_p), and (T_{in} and T_{out}) are the mass flow rate, specific heat, and inlet/outlet temperature of the HTF, respectively.

In the transient process, the accumulative energy is realized or acquired by water ($Q_{ch\ \&\ dis}$) and the PCM ($Q_{pcm,\ ch\ \&\ dis}$) as opposed to the steady-state process. This part of heat exchange can be expressed as below:

$$Q_{H.E,ch} = M_{H.E} C_{p,H.E} (T_{end} - T_{ini}) \quad (13)$$

$$Q_{H.E,dis} = M_{H.E} C_{p,H.E} (T_{ini} - T_{end}) \quad (14)$$

Where ($M_{H.E}$), and ($C_{p,H.E}$) are the mass, and specific heat of the exchanger, respectively, and (T_{ini} and T_{end}) are the start/end temperature of the PCM during the process.

Furthermore, the accumulative energy exchangeable with PCM ($Q_{pcm,\ ch\&dis}$) can be written as follows:

$$Q_{pcm,ch\&dis} = Q_{ch\&dis} - Q_{H.E,ch\&dis} \quad (15)$$

The thermal performance of LHTES can be described as follow:

$$\eta_{theory} = \frac{Q_{pcm,ch\&dis}}{Q_{max,ch\&dis}} \quad (16)$$

The maximum quantity of energy (Q_{max}) through the charging and discharging process obtained from PCM can be written as:

$$Q_{max,ch} = M_{pcm}\left[C_{p,pcm}(T_{ini} - T_{solidus}) + L + C_{p,pcm}(T_{end} - T_{liquidus})\right] \quad (17)$$

$$Q_{max,disch} = M_{pcm}\left[C_{p,pcm}(T_{ini} - T_{liquidus}) + L + C_{p,pcm}(T_{end} - T_{solidus})\right] \quad (18)$$

where (M_{PCM}), ($Cp_{,PCM}$), (L), and ($T_{solidus}$ & $T_{liquidus}$) are the mass, specific heat, latent heat, and solidus/liquidus temperature of the PCM, respectively.

2.5 Nusselt Number

Nusselt number is a parameter that is used to find out which heat transfer mechanism is dominant. It is expressed as follows **(Kousha et al., 2019)**:

$$\overline{Nu} = \frac{\bar{h}(t) L_c}{k_{pcm}} \quad (19)$$

$$L_c = R_{shell} - R_t \quad (20)$$

$$\bar{h}(t) = \frac{\dot{Q}(t)}{A_w(T_w - T_m)} \quad (21)$$

$$\dot{Q}(t)_{ch/dis} = \dot{m}c_p(T_{out} - T_{in}) \quad (22)$$

$$A_w = 2\pi R_t \times L \quad (23)$$

$$T_w = \frac{T_{in}+T_{out}}{2} \quad (24)$$

Where h is heat transfer coefficient, L_c is the characteristic length, $\dot{Q}$ is the heat transfer rate between HTF and PCM, A_w heat transfer area, T_w wall temperature, T_m is the melting temperature, and k_{pcm} is the thermal conductivity of PCM.

3. Numerical Procedure

In the present study, the computational during solidification is performed using ANSYS fluent. It is a commercial software program. The boundary condition of the shell's outer surface and both ends were assumed adiabatic. During the discharge process, the PCM was initially set in the liquid phase with a temperature of 340 K for both cases, case1 and case2. The HTF in laminar flow with Reynolds number of 1600 and temperature at inlet has been set with 296 K. The SIMPLE algorithm is used for the pressure velocity coupling, the PRESTO scheme is used for the pressure correction equation, and second-order upwind is used for momentum and energy.

4. Model verification

For the current simulation, the geometry was adopted in shell and tube as cleared in **Figure 2**. The mesh independence has been verified, and **Figure 3** illustrates the mesh generation. Five grids were investigated to validate the mesh independent of the grid size for the numerical solution, as shown in **Figure 4**. It is found that element 395232 has the best result and is short and time-consuming. The time steps of the liquid fraction were examined, and found that 1sec was the most accurate and time-consuming. The simulation was compared with numerical data **(Liu et al., 2020)** during the discharge process as shown in **Figure 5**.

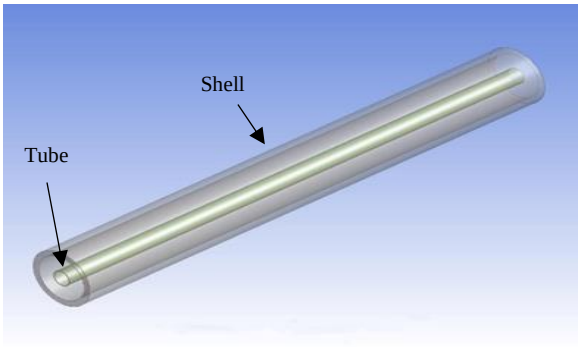

Figure 2 Geometry of the study

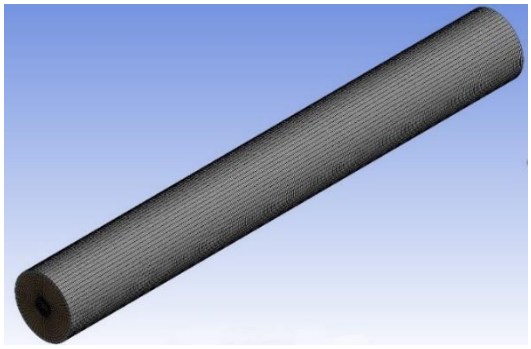

Figure 3 Mesh generation

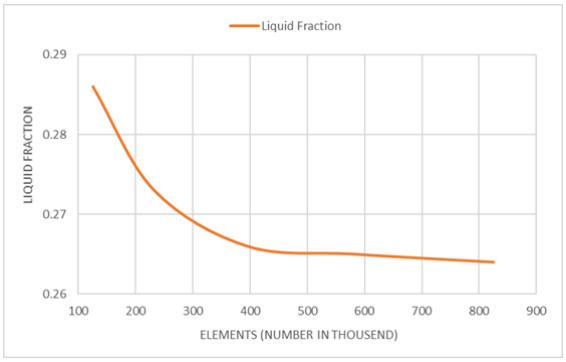

Figure 4 Analysis of mesh number

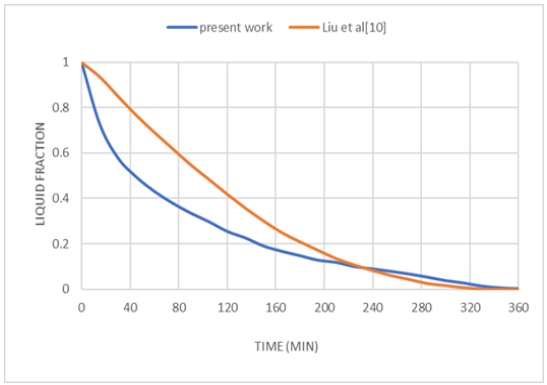

Figure 5 comparison curve of liquid fraction with numerical data Liu et al

5. RESULTS and DISCUSSION

Thermal behaviour and thermal performance of LHTESS of horizontal concentric shell and tube heat exchanger were performed numerically. The effect of the thermal conductivity of the PCM on the performance during the discharge process has been analyzed. Two organic material of paraffin wax with different thermal conductivity (case 1 and case 2) is used as a PCM. Water as HTF of flow

rate 2l/min and constant temperature of 296 K has been used. The initial temperature of PCMs for both cases has been settled at 340 K at the beginning of the solidification process. The numerical simulation results were compared to each other for both cases (case1 and case2), as illustrated in the following section.

Figure 6 and **Figure 7** show the contours of PCMs liquid fraction for case1, and case2 shows the evolution of the solid phase rate and the variation of liquid fraction with time. At the begging of the discharge process, heat transfer is dominated by natural convection in the LHTES unit. As a result, sensible heat is removed from the PCM and dropping the temperature quickly. A layer of solidified PCM surrounding the outer surface of the HTF tube behaves like an insulation material. Hence, attributable to low thermal conductivity. Also, Figure 6 and Figure 7 show the discharge process moves up, and solidification is faster in the lower part of the horizontal LHTES unit. This behaviour is due to the buoyancy and the convective heat transfer in the solid-liquid phase **(Seddegh et al., 2016)**. It is evident that there is a difference in liquid fraction and temperature between case1 and case 2, as shown in **Fig. 6 and 7**. The solidification behaviour of case 2 is enhanced compared to case1 due to the high thermal conductivity of the PCM of case 2. From the contours result, it is clear that the discharge process is affected by the thermal conductivity because the heat transfer is dominated by thermal conduction in the solidification process. The solidified part of the two cases after 30 min is almost the same, with little difference in liquid fraction for case 2, which is slightly less than case 1 as shown in **Fig. 6 and 7**. After 60 min, the difference in liquid fraction increased, and this difference increased with time until case 2 reached 0.174 liquid fraction after 120 minutes whereas case1 reached 0.266 after 145 minutes.

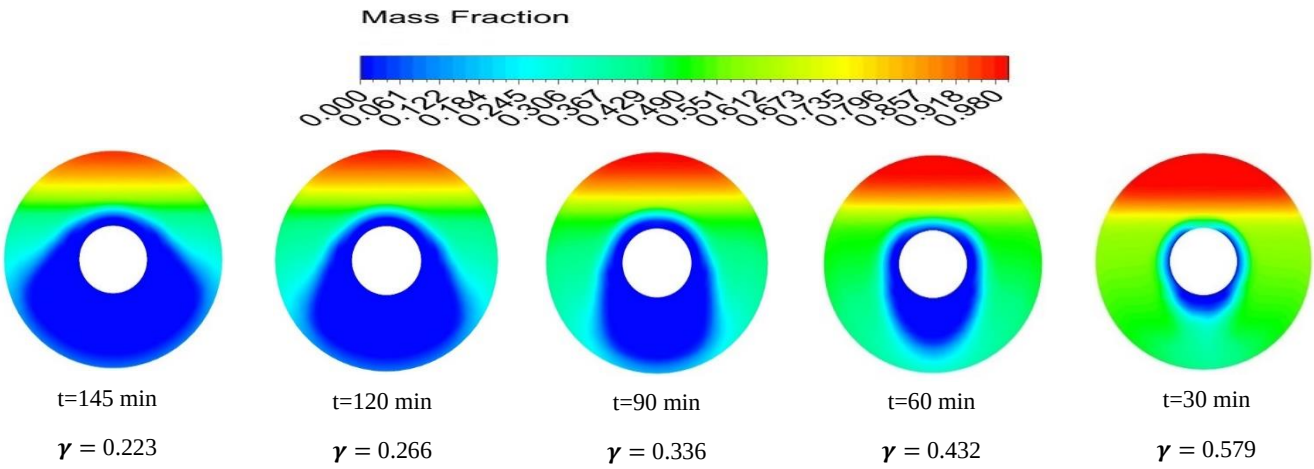

Figure 6 Liquid fraction Contours of case1

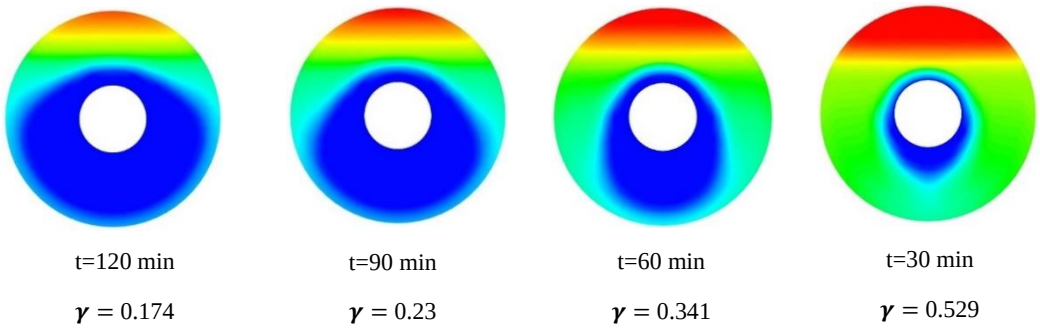

Figure 7 Liquid fraction Contours of case 2

Figure 8 and **Figure 9** show the contours of the temperature gradient at the specified time where the evolution in temperature during the solidification process is evident. The temperature in case 2 is significantly lower than in case1 at different times. This difference in temperature because case 2 has a higher thermal conductivity which accelerates the solidification process compared to case1. It can be seen that the change in temperature for case2 is 319.1 K after 120min while it is 322.6 K after 145 min.

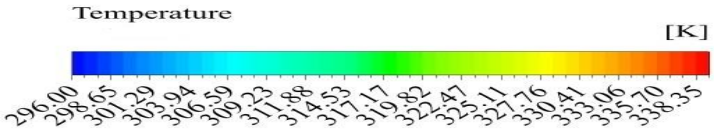

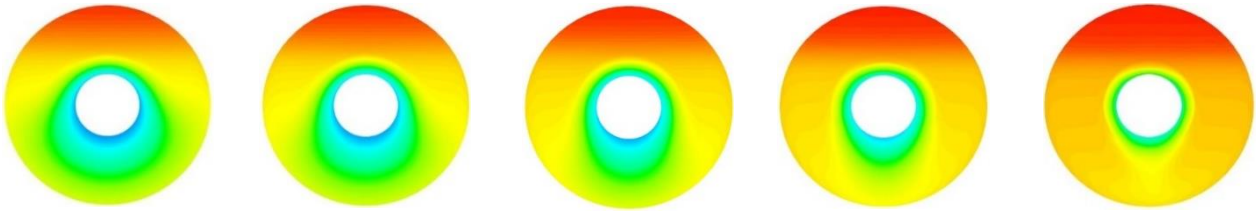

t=145 min ***T*** =322.6 | t=120 min ***T*** =323.9 | t=90 min ***T*** =325.8 | t=60 min ***T*** = 328.2 | t=30 min ***T*** = 331.2

Figure 8 Temperature gradient Contours of case1

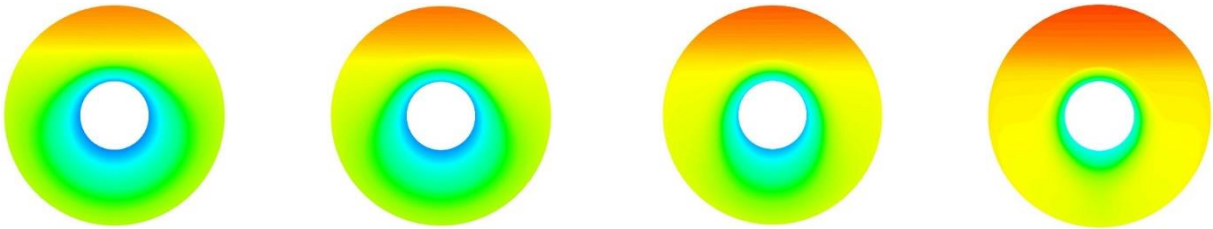

t=120 min ***T*** =319.1 | t=90 min ***T*** =320.5 | t=60 min ***T*** = 323.3 | t=30 min ***T*** =327.4

Figure 9 Temperature gradient Contours of case 2

The temporal variation of the liquid fraction and average temperature during the solidification process of both PCMs were demonstrated in **Figure 10** and **Figure 11**, respectively. When thermal conductivity increases, the time required for full discharge decreases. High thermal conductivity means a high-temperature difference between PCMs, which leads to increases in the heat transfer and makes the discharge process shorter.

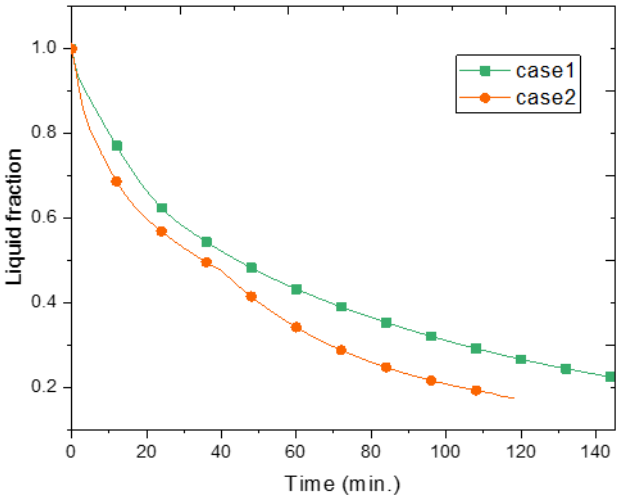

Figure 10 Liquid Fraction Profile

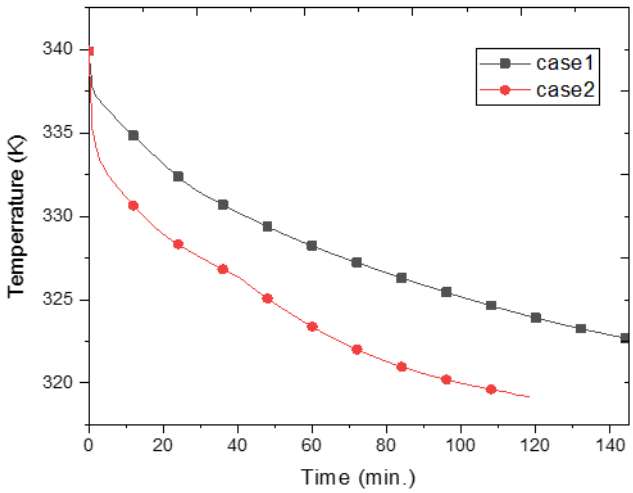

Figure 11 Temperature distribution Profile

Figure 12 represented the accumulative energy transferred from PCM to HTF. It can be seen that the cumulative energy of case2 is higher than case1. At the beginning of the discharge process, the natural convection dominated the temperature of the PCM drop near the HTF tube, forming a layer around the tube. The layer around the tube works as insulation material, and the heat conduction is dominated in this stage. In heat conduction, thermal conductivity has a significant role. Generally, the main drawback of PCM is low thermal conductivity. If the thermal conductivity is high, that means a higher heat transfer rate, as seen in case 2. Due to case 2 having higher thermal conductivity than case1, it has higher cumulative energy.

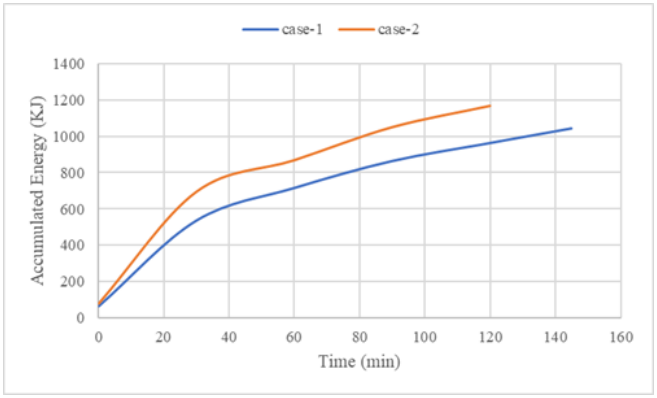

Figure 12 Accumulated Energy

Figure 13 shows the variation of the Nusselt number versus time which represents a criterion to find out which heat transfer mechanism dominates. It can be noticed that the average Nusselt number has the maximum value at the beginning for both cases. However, case2 has a higher average Nusselt number than case1. This difference is due to the thermal conductivity, which affects the number. The descent in the number due to heat conduction is dominant and a layer of PCM is formed around the tube. The decrease in the number continues until the minimum value reaches the end of the solidification process and the PCM has fully solid. The performance of LHTESS increased when the average temperature and liquid fraction decreased. The theoretical efficiency during the discharge process for case 2 is 63.2%, whereas for case1 is 54.6%, and the time required for the whole solidification process becomes shorter by 20%.

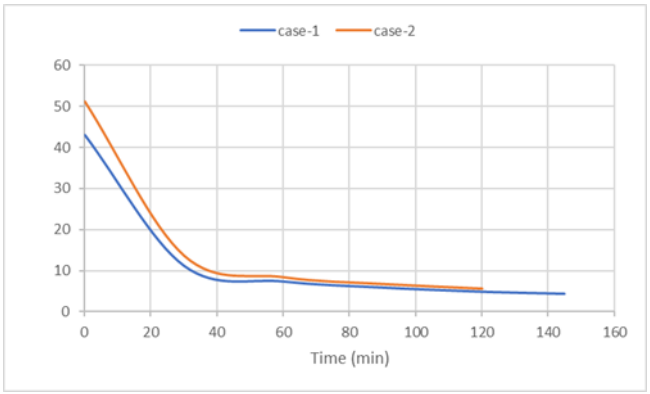

Figure 13 Variation of Average Nusselt number

Figure 14 and **Figure 15** show a comparison between case 1 and case 2 in average temperature and liquid fraction respectively at the specified time. To verify the result of the present study, a comparison was made with previous research. The liquid fraction profiles in Figure 10 agreed with the result of **(Mahdi and Nsofor, 2016),** who studied the performance of the solidification process. Also, the result showed a good agreement with the result of **(Khatibi et al., 2021),** who optimized and investigated the performance of the solidification behavior.

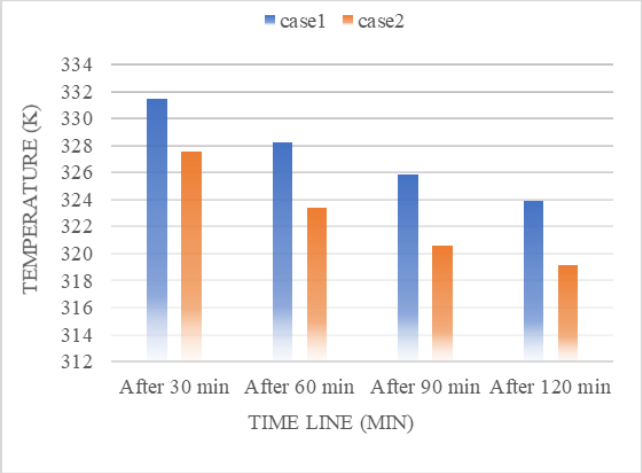

Figure 14 Comparison of the temperature gradient at the specified time of both cases

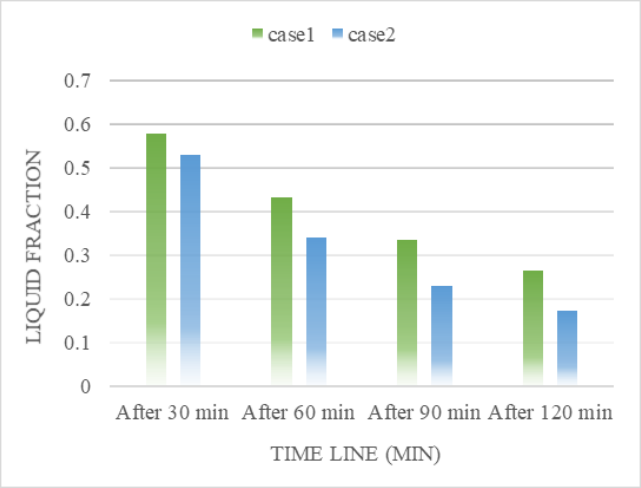

Figure 15 Comparison of the liquid fraction at the specified time of both cases

6. CONCLUSIONS

In the present study, the effect of the thermal conductivity of PCM on the performance of LHTESS has been investigated. A horizontal concentric shell, tube heat exchanger as LHTES, and two types of PCMs with different thermal conductivity were used. The analysis result of the two PCMs was compared during the solidification process. The conclusion is summarized below:

- During the discharge process, heat transfer in case 2 (the PCM with high thermal conductivity) is more effective than in case1(the PCM with low thermal conductivity), and theoretical efficiency for case 2 is more efficient than in case1 by 13.6%.
- Comparing the results leads to that the solidification time is reduced from 145min for case1 to 120min in case2. The ratio of the decrease of two cases is 20%. Hence, high thermal conductivity can notably improve the performance of LHTESS.
- Due to the heat conduction being dominant by which the thermal conductivity plays a significant role, the accumulated energy of case2 is higher than that of case1.
- The average Nusselt number has the maximum value at the beginning of the process and has a higher value for case2.
- The solidification time of PCM is significantly affected by the thermal conductivity of PCM, therefore, the solidified time decreases with an increase in thermal conductivity.

Nomenclature	
C_p	Specific heat (J/kg·K)
D_{in}	Inner diameter of the shell
d_{in}	Inner diameter of the tube
H	Total enthalpy (J/kg)
h	Heat transfer coefficient or enthalpy (W/m2 ・K or J/kg)
k	Thermal conductivity (W/m·K)
L	Latent heat (J/kg)
$\boldsymbol{M_{H.E}}$	Mass of heat exchanger (kg)
$\boldsymbol{M_{pcm}}$	Mass of the PCM
Q	Accumulative energy
$\boldsymbol{Q_{H.E}}$	Energy of heat exchanger
Q_{max}	Maximum energy
$\boldsymbol{Q_{pcm}}$	Energy of phase change material
q	Instantaneous energy
S	Source term
T	Temperature (K)
$\boldsymbol{T_{in}}$	Inlet temperature (K)
$\boldsymbol{T_{out}}$	Outlet temperature (K)
$\boldsymbol{T_{end}}$	Temperature of the end process (K)
$\boldsymbol{T_{ini}}$	Initial temperature of the process (K)
$\boldsymbol{T_{solidus}}$	Solidus temperature (K)
$\boldsymbol{T_{liquidus}}$	Liquidus temperature (K)
$\boldsymbol{\Delta t}$	Time (s)
$\boldsymbol{\gamma}$	Liquid fraction factor
$\boldsymbol{\dot{m}}$	Mass flow rate (kg/s)
Greek letter	
μ	Dynamic viscosity (kg/m·s)
η	Efficiency
ρ	Density (kg/m^3)
$\boldsymbol{\beta}$	Volumetric expansion coefficient (1/K)
$\boldsymbol{\varepsilon}$	Numerical constant
Dimensionless	
Re	Reynolds number
Subscript	
ch&dis	Charge and discharge
end	End
H.E	Heat exchanger
in	Inlet
in	Inner
ini	Initial
max	Maximum
Mush	Mushy zone
out	Outlet
pcm	Phase change material
Ref	Reference

REFERENCES

Al-Abidi, A. A., Mat, S., Sopian, K., Sulaiman, M. Y., and Mohammad, A. T., 2013. Internal and external fin heat transfer enhancement technique for latent heat thermal energy storage in triplex tube heat exchangers, In *Applied Thermal Engineering* (Vol. 53, Issue 1, pp. 147–156). https://doi.org/10.1016/j.applthermaleng.2013.01.011.

Kadim, B., et al., 2015. Experimental Study on the Effect of Using Metallic Brushes on the Charging Experimental Study on the Effect of Using Metallic Brushes on the Charging and Discharging Time of Thermal Energy Storage Unit. *21*(December), 1–15.

Bhagat, K., Prabhakar, M., and Saha, S. K., 2018. Estimation of thermal performance and design optimization of finned multitube latent heat thermal energy storage, *Journal of Energy Storage*, *19*, 135–144. https://doi.org/https://doi.org/10.1016/j.est.2018.06.014

Fathi, M. I., and Mussa, M. A., 2021. Experimental study on the effect of tube rotation on performance of horizontal shell and tube latent heat energy storage, *Journal of Energy Storage*, *39*(11). https://doi.org/10.1016/j.est.2021.102626

Hosseini, M. J., Rahimi, M., and Bahrampoury, R., 2014. Experimental and computational evolution of a shell and tube heat exchanger as a PCM thermal storage system, In *International Communications in Heat and Mass Transfer* (Vol. 50, pp. 128–136). https://doi.org/10.1016/j.icheatmasstransfer.2013.11.008

Joudi, K., and Taha, A., 2012. Simulation of Heat Storage and Heat Regeneration in Phase Change Material. *Journal of Engineering*, *18*(9). http://www.coeng.uobaghdad.edu.iq/uploads/theses/mech/Ahmed-Kasim.pdf.

Khatibi, M., Nemati-Farouji, R., Taheri, A., Kazemian, A., Ma, T., and Niazmand, H., 2021. Optimization and performance investigation of the solidification behavior of nano-enhanced phase change materials in triplex-tube and shell-and-tube energy storage units, *Journal of Energy Storage*, *33*(June), 102055. https://doi.org/10.1016/j.est.2020.102055.

Kousha, N., Rahimi, M., Pakrouh, R., and Bahrampoury, R., 2019. Experimental investigation of phase change in a multitube heat exchanger, *Journal of Energy Storage*, *23*, 292–304.

https://doi.org/10.1016/j.est.2019.03.024.

Kuboth, S., König-Haagen, A., and Brüggemann, D., 2017. Numerical analysis of shell-and-tube type latent thermal energy storage performance with different arrangements of circular fins, In *Energies* (Vol. 10, Issue 3). https://doi.org/10.3390/en10030274.

Li, Z., and Wu, Z. G., 2015. Analysis of HTFs, PCMs and fins effects on the thermal performance of shell-tube thermal energy storage units, *Solar Energy*, *122*, 382–395. https://doi.org/10.1016/j.solener.2015.09.019.

Liu, M., Riahi, S., Jacob, R., Belusko, M., and Bruno, F. (2020). Design of sensible and latent heat thermal energy storage systems for concentrated solar power plants: Thermal performance analysis, *Renewable Energy*, *151*, 1286–1297. https://doi.org/10.1016/j.renene.2019.11.115.

Mahdi, J. M., and Nsofor, E. C., 2016. Solidification of a PCM with nanoparticles in triplex-tube thermal energy storage system, *Applied Thermal Engineering*, *108*, 596–604. https://doi.org/10.1016/j.applthermaleng.2016.07.130.

Nóbrega, C. R. E. S., Ismail, K. A. R., and Lino, F. A. M., 2021. Thermal performance of bare and finned tubes submersed in nano-PCM mixture, *Journal of the Brazilian Society of Mechanical Sciences and Engineering*, *43*(1), 1–14. https://doi.org/10.1007/s40430-020-02740-5.

Parsazadeh, M., and Duan, X., 2018. Numerical study on the effects of fins and nanoparticles in a shell and tube phase change thermal energy storage unit, *Applied Energy*, *216*, 142–156. https://doi.org/https://doi.org/10.1016/j.apenergy.2018.02.052.

Pu, L., Zhang, S., Xu, L., Ma, Z., and Wang, X., 2021. Numerical study on the performance of shell-and-tube thermal energy storage using multiple PCMs and gradient copper foam, *Renewable Energy*, *174*, 573–589. https://doi.org/10.1016/j.renene.2021.04.061.

Seddegh, S., Wang, X., and Henderson, A. D., 2016. A comparative study of thermal behaviour of a horizontal and vertical shell-and-tube energy storage using phase change materials, *Applied Thermal Engineering*, *93*, 348–358. https://doi.org/10.1016/j.applthermaleng.2015.09.107.

Shi, E., Ahangar Zonouzi, S., Aminfar, H., and Mohammadpourfard, M., 2020. Enhancement of the performance of a NEPCM filled shell-and-multi tube thermal energy storage system using magnetic field: A numerical study, *Applied Thermal Engineering*, *178*, 115604. https://doi.org/10.1016/j.applthermaleng.2020.115604.

Tao, Y. B., Liu, Y. K., and He, Y. L., 2019. Effect of carbon nanomaterial on latent heat storage performance of carbonate salts in horizontal concentric tube, *Energy*, *185*, 994–1004. https://doi.org/10.1016/j.energy.2019.07.106.

Yang, X., Lu, Z., Bai, Q., Zhang, Q., Jin, L., and Yan, J., 2017. Thermal performance of a shell-and-tube latent heat thermal energy storage unit: Role of annular fins, *Applied Energy*, *202*, 558–570. https://doi.org/https://doi.org/10.1016/j.apenergy.2017.05.007.